Environmental Science Nano

Selective Imaging of Diamond Nanoparticles within Complex Matrices using Magnetically Induced Fluorescence Contrast

Journal:	*Environmental Science: Nano*
Manuscript ID	EN-ART-09-2019-001008.R1
Article Type:	Paper

Environmental Significance Statement:

To understand the impact of nanomaterials released into the environment it is essential to identify the location of nanoparticles with complex environmental matrices, including within organisms of environmental relevance. This work demonstrates the utility of a differential imaging method that leverages the high stability and unique fluorescent properties of diamond nanoparticles containing nitrogen vacancy centers to enable selective imaging of nanoparticles ingested *by C. elegans* as a model organism. Broader use of this approach would enable selective visualization of nanoparticles in a wide range of matrices and organisms of environmental significance that exhibit high levels of background fluorescence and scattering. These techniques may ultimately open the door for an increased understanding of the long-term environmental fate of nanomaterials.

ARTICLE

Selective Imaging of Diamond Nanoparticles within Complex Matrices using Magnetically Induced Fluorescence Contrast

Received 00th January 20xx,
Accepted 00th January 20xx

DOI: 10.1039/x0xx00000x

Zachary R. Jones[a], Nicholas J. Niemuth[b], Margaret E. Robinson[a], Olga A. Shenderova[c], Rebecca D. Klaper[b], and Robert J. Hamers[a]*

The use of fluorescence microscopy to study fate and transport of nanoparticles in the environment can be limited by the presence of confounding background signals such as autofluorescence and scattered light. The unique spin-related luminescence properties of nitrogen vacancy (NV) centers in diamond nanoparticles (NVND) enable new types of imaging modalities such as selective imaging of nanoparticles in the presence of background fluorescence. These techniques make use of the fact that the spin properties, which affect the fluorescence of NV centers, can be modulated using applied magnetic or radio-frequency fields. This work presents the use magnetic fields to modulate the fluorescence of NVND for background-subtracted imaging of nanoparticles ingested by a model organism, *C. elegans*. With the addition of modest time-modulated magnetic fields from an inexpensive "hobby" electromagnet, the fluorescence of 40 nm NVND can be modulated by 10% in a widefield imaging configuration. Herein, differential magnetic imaging is used to image and to isolate the fluorescence arising from nanodiamond within the gut of the organism C. elegans. This method represents a promising approach to probing the uptake of nanoparticles by organisms and to assessing the movement and interactions of nanoparticles in biological systems.

Introduction

A major challenge in characterizing the movement and accumulation of nanomaterials in the environment is the difficulty of selectively detecting nanoparticles in complex matrices such as biological organisms due to the presence of autofluorescence, scattering, and other emission sources.[1-7] Several approaches to overcoming this problem have included the use of hyperspectral imaging,[8] two-photon excitation,[9] and upconverting nanoparticles.[10] Detection of nanomaterials at low concentrations and over after extended periods of time, which is important for understanding potential chronic effects of nanoparticle exposure in multicellular organisms, is particularly challenging due to chemical and/or photochemical degradation of many types of nanoparticles such as semiconducting quantum dots.[11-13] Thus, there remains a need for selective detection of nanoparticles with stable chemical and optical properties in environmental and biological matrices.

Nitrogen vacancy (NV) centers in diamond have recently emerged as a highly stable chromophore with unusual properties that make it attractive for imaging[14-16] and new applications such as quantum computing,[17] and quantum sensing.[18-22] NV centers consist of a solid-state defect in which a nitrogen atom substitutes for carbon atom within the diamond lattice with an adjacent carbon vacancy. The electrons of the nitrogen "lone pair" orbital and the adjacent carbon atoms give rise to a highly stable optically active chromophore. Diamond nanoparticles containing NV centers are of particular interest for the investigation of nanoparticle interactions in the environment and in living organisms because NV centers have high brightness with nearly infinite photostability and resistance to bleaching.[10, 15, 16, 23-27] In addition, the surrounding diamond has very stable surface chemistry even in complex matrices.[28, 29] A particularly important property of NV centers that is relevant to selective detection arises from the fact that they have a triplet ground-state electronic configuration that leads to unique optical properties, including the ability to modulate the intensity of NV fluorescence by applying a weak radiofrequency field and/or a static magnetic field. Since typical chromophores and autofluorescence are unaffected by these fields, selective modulation of the NV fluorescence using RF or static magnetic fields can be used to isolate the NV fluorescence from competing background signals.

Here, we report studies aimed at understanding how the selective modulation of NV fluorescence in diamond nanoparticles depends on experimental parameters important for widespread adoption of this method, and we demonstrate the use of differential magnetic-field imaging to directly image the spatial distribution of NV-containing nanoparticles ingested by a model organism, *Caenorhabditis elegans (C. elegans)*. Our studies show that selective contrast between nanodiamond and non-diamond background such as autofluorescence and scattering of the *C. elegans* can be achieved using a small,

[a] Department of Chemistry, University of Wisconsin-Madison, 1101 University Avenue, Madison, WI 53706, United States
[b] Great Lakes Freshwater Research Institute, University of Wisconsin-Milwaukee, 600E Greenfield Ave. Milwaukee, WI 53204, United States
[c] Adámas Nanotechnologies, 8100 Brownleigh Drive, Raleigh, North Carolina 27617, United States

inexpensive electromagnet without the use of microwaves or other radio-frequency fields. Analysis of the signal-to-noise of intensity profiles across a *C. elegans* organism shows that NV center fluorescence can be reliably distinguished from background fluorescence, with differential images leading to signal-to-noise ratios (S/N) of >13 with imaging times of less than 10 minutes. In addition, we explore how the parameters of nanodiamond size, magnetic field strength, illumination intensity, and emission wavelength can be tuned to improve the magnet on vs. magnet off fluorescence contrast. A key feature of NV nanodiamond is that the fluorescent NV center is buried within a chemically stable nanodiamond core. As a result, the chemical and optical properties are highly stable under all conditions. This stability allows NV nanodiamond to be used to study transport and bioaccumulation over long timescales that are not accessible to other fluorescent nanoparticles. The use of differential imaging with and without magnetic fields provides a simple approach to imaging NV nanodiamond that can be easily replicated in other laboratories equipped with fluorescence microscopes and used to selectively detect nanoparticles within multicellular organisms.

Introduction to NV Center Optical Properties

The optical properties of NV centers are well understood based on studies in single crystal diamond. [22, 30, 31] However, the rates that define the NV center spin dynamics, giving rise to selective modulation, are affected by proximity to surfaces and therefore vary depending on properties such as nanoparticle size. We first introduce a short explanation of the spin dynamics that underlie the selective modulation properties. The ground-state electronic configuration of the NV center (^{3}A) in its negative charge state (the form most useful for quantum-based sensing) has two co-parallel electron spins, giving rise to a total spin S=1 that has three possible orientations with respect to the symmetry axis of the NV center. These three spin orientations give rise to three magnetic sub-level states denoted by m_s= +1, 0, and -1. Two of these states ($m_s = \pm1$) are equal in energy and correspond to having the total spin S oriented parallel or anti-parallel to the N-V axis, while a third state ($m_s = 0$) has the spin S oriented perpendicular to this axis. In the absence of a magnetic field, the $m_s = \pm1$ states have identical energies but the $m_s = 0$ state is slightly different in energy. The resulting energy gap (a zero-field splitting) can be bridged using a microwave field at a frequency of 2.87 GHz. The NV spins have a coherence time that is long (microseconds) compared to their fluorescence lifetimes. When electrons are optically excited from the ground (^{3}A) state to the excited (^{3}E) using 532 nm light, their spin orientation is usually retained, but some electrons undergo a spin-dependent intersystem crossing to the singlet $^1A_2$ state. The overall rates of the excitation, fluorescence, and relaxation processes result in the selective pumping of spins into the $m_s = 0$ state. The fluorescence intensity depends on the distribution of spins among the $m_s = 0$ and ±1 sublevels, yielding higher fluorescence intensity when the spin population is in $m_s = 0$.

Because of these spin-dependent optical properties, intentional manipulation of the populations of the different spin states can be used to selectively modulate the fluorescence intensity of NV centers in nanodiamond. In one approach, optically detected magnetic resonance (ODMR)[22, 30] the spin spates are manipulated by applying a radio-frequency field at 2.87 GHz, resonant with the energy gap between the $m_s = 0$ and $m_s = \pm1$ states. Differential imaging of on-resonance and off-resonance microwaves can selectively image NV-nanodiamonds,[32, 33] but the maximum contrast available in this approach is small (typically ~5% using nanodiamond). An alternative approach, depicted schematically in **Figure 1a**, is to modulate the NV fluorescence intensity using an applied magnetic field, which reorients the axis of quantization and mixes the spin states, reducing the spin polarization and ultimately decreasing the fluorescence intensity.[34-38] Initial studies using static magnetic fields showed that subtracting images in the absence and presence of a magnetic field yielded fluorescence contrast in chloroplasts,[39] neuronal cultures grown with nanodiamond,[40] lymph nodes in mice,[37] and stem cells in miniature pigs.[41] These previous studies explored imaging of nanoparticles that were directly injected into tissues or other organisms and demonstrated that acquiring images in the presence and absence of magnetic fields yields a contrast of ~6%. [37] These prior studies suggest that the use of differential magnetic imaging to isolate nanodiamond fluorescence in the presence of autofluorescence and other non-diamond emission could help to locate and track nanodiamond in complex systems. [37, 39, 40] However, they did not conduct systematic studies to identify how the achievable contrast from NV diamond nanoparticles varied with experimentally accessible parameters such as nanodiamond diameter, or magnetic field strength, parameters important to understanding how to adopt these techniques more widely. Our results show modulated magnetic field differential imaging using commercially available NV nanodiamond and a small electromagnet can yield magnetic contrast up to 20%. This approach provides a pathway to selective detection of nanoparticles and their location within multicellular organisms after uptake from the surrounding matrix via natural biological pathways such as ingestion.

Materials and Methods

Fluorescence Measurements

All images were collected using a custom-built inverted microscope shown schematically in **Figure 1b**. Fluorescence excitation is from a 532 nm continuous wave laser (Opto Engine LLC-500mW) through a stabilizer (Thorlabs Noise Eater NEL02), directed to the sample using a dichroic mirror (Semrock, FF-552-di02) and a 40x objective (Nikon PlanFluor, 40x 0.7 NA). Brightfield excitation comes from a lamp placed above the sample (Titan Tool Supply Co., FO-150). Emission and white light pass through the dichroic mirror and are directed to a tube lens (Thorlabs) forming a real image as well as line reject filter (Semrock). A pair of transfer lenses forming a 4f correlator transfer this image onto the focal plane of an electron-multiplying charge-coupled device (EMCCD, Andor IXON Ultra 888).

A removable mirror can be inserted to redirect the fluorescence to a sidearm for spectroscopic measurements via a monochromator (Andor Shamrock 193i) and an intensified charge-coupled device (ICCD) (Andor iStar). Spectra were collected using a grating with 150 lines/mm and blazed at 300 nm. Alternatively, a dichroic mirror (Semrock, FF556-SDi01) can be inserted into the sidearm to redirect the light through a bandpass filter (Newport, 10BPF25-650) to a single photon counting module (Excelitas SPCM-AQRH-14). Experiments using applied magnetic fields used an inexpensive hobby electromagnet (Uxcell, 12V 50N) placed 5 mm above the microscope stage and powered though a source meter (Keithley 2425 100W) which applied a constant voltage of either 12 V (magnet on) or 0 V (magnet off), or in some experiments constant current of 0.35 A (magnet on) or 0 A (magnet off) to the electromagnet. The strength of magnetic fields applied to the sample were measured using a gaussmeter (Magnetic Sciences Bell-5180) placing the probe at the sample position and measuring the field produced with increasing voltage applied to the magnet. Measurements at differing magnetic field strengths were performed by applying varying current to the electromagnet and calibrated using the above-described gaussmeter measurements.

Experiments were performed with size-selected nanodiamonds of 20 nm, 30 nm, and 40 nm diameter. Experiments shown here primarily used 40 nm diameter nanoparticles due to their higher contrast. Fluorescence vs. time traces under magnetic modulation were created by drying a drop of 40 NVND solution (Adamas Nanotechnologies, ND-10NV-40nm 0.1% wt) to a coverslip on a hotplate. NV center fluorescence was located using the imaging configuration described above, then directed to the single photon counting module. Photons were counted using a universal time-interval counter (Stanford Research Systems SRS620). Fluorescence was collected for 1s per data point, with 4 data points for every magnet setting (i.e. 4 points with magnet off, 4 points with magnet on). Instrument control and data collection were performed using LabView (National Instruments). Size-dependent measurements were determined by averaging fluorescence-time traces from NVND of various sizes.

Intensity dependent measurements were preformed using constant laser output power attenuated by varying degrees using neutral density filters. Laser power was measured at the sample location using a thermopile (Scientech AC2500). Highest intensities were achieved by removing the defocusing lens to reduce the spot size and area was determined by fitting the intensity profile of the illumined spot and defining area as FWHM.

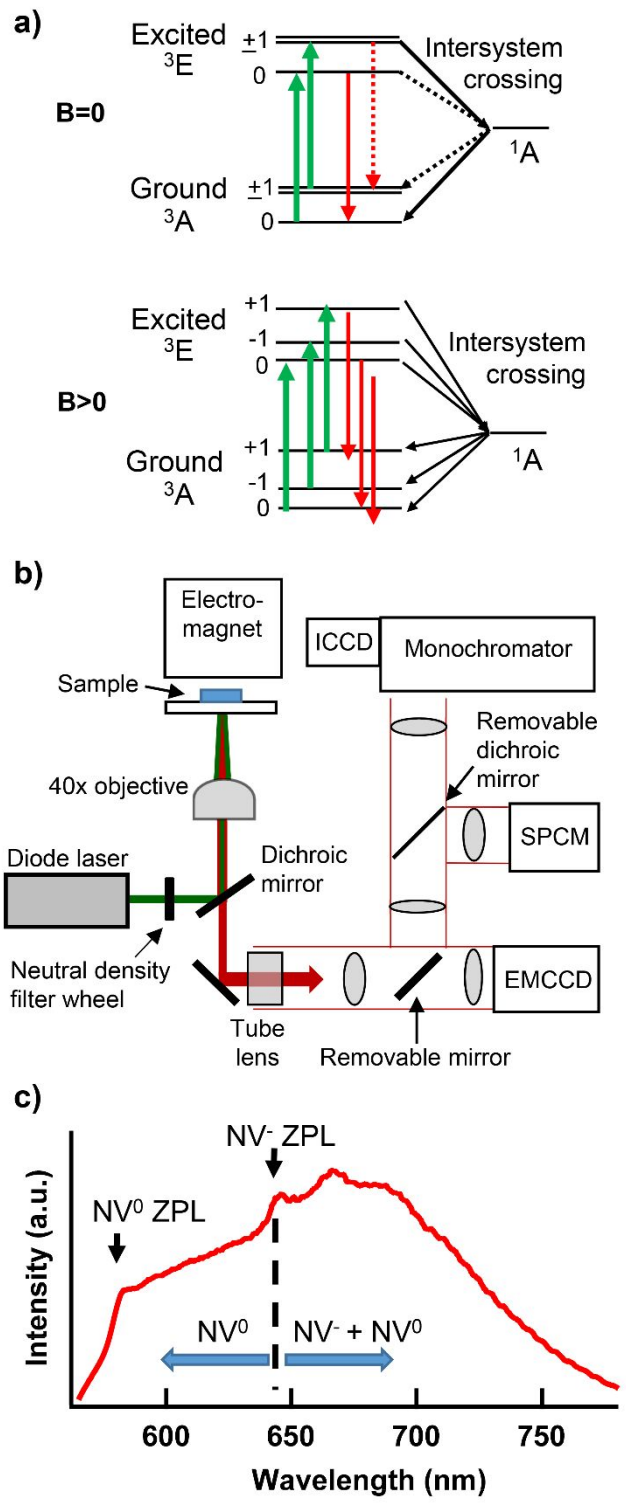

Figure 1. a) Magnetic sublevels of NV centers in the presence and absence of a magnetic field. b) Optical apparatus used in these experiments. c) Fluorescence spectrum of 40 nm NV nanodiamond

C. elegans Culture and Exposure

We obtained *C. elegans* N2 worms and OP50 *E. coli* from the Caenorhabditis Genetics Center (University of Minnesota, Minneapolis, MN). Worms were cultured at 20 °C on OP50-seeded solid nematode growth medium (NGM) plates following protocols outlined in WormBook.[42] Synchronized L1 (first larval stage) larvae were generated for exposures using Wormbook bleaching Protocol 6 and synchronized overnight without food on an NGM plate. Briefly, *C. elegans* stock was exposed to hypochlorite solution which kills bacteria and worms but not eggs. Remaining eggs were then incubated on an NGM plate without food overnight to synchronize hatched larvae at the L1 stage. NV nanodiamond exposure solutions were created by combining 500 µL NVND solution (Adamas ND-10NV-40nm

0.1% wt.) in water (500 μL sterile water for controls) with concentrated OP50 (500 μL) and vortexing to mix for a final nanodiamond exposure concentration of 0.5 mg/mL. 100 mm NGM exposure plates were created by adding exposure solution (1 mL) to each plate and drying plates overnight in a fume hood. Starved L1 larvae were washed from their plate using M9 media,[42] pelleted at 2500*g* 20 °C for 1 min, and resuspended in M9 at 10 worms per μL. Approximately 1500 larvae (150 μL) were then added to each exposure plate.

C. elegans Fixation and Imaging

C. elegans larvae were washed from exposure plates with M9 buffer after 24 hr of nanodiamond exposure, pelleted and washed 3 times with M9, fixed in 4% paraformaldehyde for 45 min, and then pelleted and rinsed 3 times with 1x PBS and stored at 4 °C. Fluorescence imaging of exposed and fixed *C. elegans* was performed by vortexing the sample briefly to disperse settled organisms before adding 10 μL of sample to a glass coverslip. Images were collected and converted using a custom LabView program. Bright-field images were collected using a 10 ms exposure time and accumulated over 100 exposures. Florescence images were collected using 500 ms exposure time with EMCCD gain set to 50 and accumulated over 10 exposures. As photo bleaching of organism autofluorescence was observed over the course of imaging, fluorescence image series were collected alternately with the magnet on and magnet off, acquiring a total of 20 images (10 with magnet on, 10 with magnet off).

Results and Discussion

Magnetic Field Control of Fluorescence Intensity

Figure 1b shows the experimental apparatus used here. Briefly, it is a custom-built inverted optical microscope in which fluorescence emission can be directed to multiple detectors to perform imaging, spectroscopy, and time-resolved measurements on a single sample in the presence and absence of an applied magnetic field. Details of the apparatus and components are given in the Materials and Methods section.

Figure 1c shows a fluorescence spectrum of 40 nm diamond nanoparticles. Consistent with prior studies, the room-temperature emission from NV centers in the negative charge state (NV^-) exhibits a zero-phonon line at 638 nm with a broad phonon-assisted sideband extending to about 800 nm. This NV^- charge state is the state that is accessible for magnetic contrast imaging due to the spin triplet resulting from two unpaired electrons within the vacancy.[30] The neutral NV^0 charge state has a zero-phonon emission at 575 nm and a phonon assisted sideband extending to ~700 nm but lacks the triplet electron spin that enables spin polarization in NV^-. Prior studies have shown that as nanoparticle size decreases, space-charge effects at the nanodiamond surface lead to a gradual shift in charge state from NV^- to NV^0.[7, 33, 43, 44] This shift in charge state has the effect of reducing the available contrast in ODMR and other spin-dependent measurements, since NV^0 fluorescence overlaps that of NV^- while only NV- emission exhibits intensity changes with applied microwave or magnetic fields.

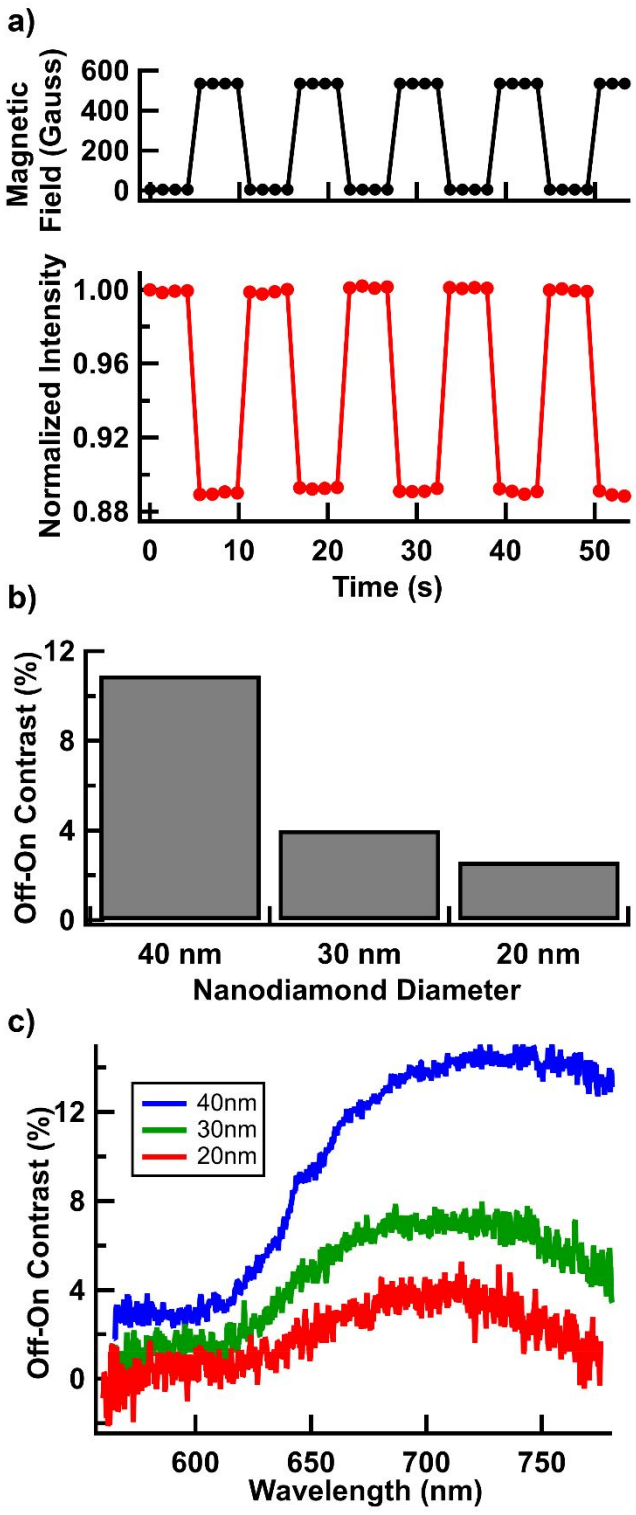

Figure 2. a) Dependence of fluorescence emission on B=530 Gauss magnetic field. b) Contrast as a function of nanoparticle diameter, for B=530 G. c) Contrast as a function of emission wavelength for varying nanodiamond diameters.

To characterize the contrast associated with the application of a magnetic field, we directed the NVND fluorescence onto a Single Photon Counting Module (SPCM) using a band-pass filter centered at 650 nm with full-width at half-maximum of 25 nm.

We first characterized the magnetic field-induced contrast in samples of NV nanodiamond deposited onto a glass coverslip. Using a custom LabView program, we modulated the current applied to an electromagnet, and thereby the magnetic field, in time as is shown in **Figure 2a** (top) while measuring the corresponding changes in fluorescence intensity. Figure 2a (bottom) shows corresponding time traces of the normalized NV fluorescence intensity measured at the SPCM. Under the conditions of our experiments the intensity decreases with applied magnetic field; in Figure 2a this corresponds to an approximately 10% decrease in intensity.

The attainable magnetically induced contrast also depends on the size of the diamond nanoparticles because of space-charge effects that lead to a larger fraction of NV centers in the neutral charge state, which fluoresces in the spectral range of interest.[7, 43, 44] In addition, spin centers at the nanodiamond surface can reduce the degree of spin polarization. **Figure 2b** shows the contrast averaged over repeated on-off cycles of the magnetic field for 3 nanodiamond sizes. Magnetically induced contrast is clearly visible with 20 nm diameter nanodiamonds, increasing significantly as the nanoparticle diameter increases to 30 nm and 40 nm diameter. Under our conditions, 10% contrast is readily achievable using randomly oriented 40 nm diameter nanoparticles.

In order to further study the response of varying sizes of NV nanodiamond to magnetic fields, we measured the wavelength dependence of magnet-induced fluorescence contrast for nanodiamond of varying sizes. **Figure 2c** shows the contrast spectra for all sizes measured. For each, the fluorescence contrast is at its maximum near 700 nm where the spectrum is dominated by NV^-. At shorter wavelengths, the percent contrast decreases, reaching its minimum in the region of the spectrum where only NV^0 contributes (575-638 nm). The spectra shown appear to decrease in percent contrast at the longest wavelengths; however, dark control spectra indicate that this is caused largely by a non-uniform background that is larger at one end of the CCD array. This background has the most effect at lower signal intensities which explains the more dramatic decrease in 30 nm and 20 nm samples which are dimmer as compared to 40 nm NVND.

This wavelength dependence demonstrates one of the mechanisms by which smaller sized nanodiamond shows reduced fluorescence contrast. The smaller fraction of NV^- to NV^0 in smaller nanodiamonds decreases the magnetically susceptible fluorescence with respect to the overall fluorescence of the nanodiamond. Another consequence of figure 2c is that for optimal fluorescence modulation in imaging, the experimental choice in filters allowing light at >700 nm is ideal. The choice in wavelength collected is, however, limited by the decreasing signal intensity at longer wavelengths which decreases signal-to-noise in the modulated fluorescence. Wavelengths near 700 nm maintain both high fluorescence intensity and large percent contrast.

Another factor that is important to consider when imaging nanodiamond using magnetic modulation is laser intensity. To understand the optimal illumination conditions for magnetic contrast imaging, we measured the achievable fluorescence

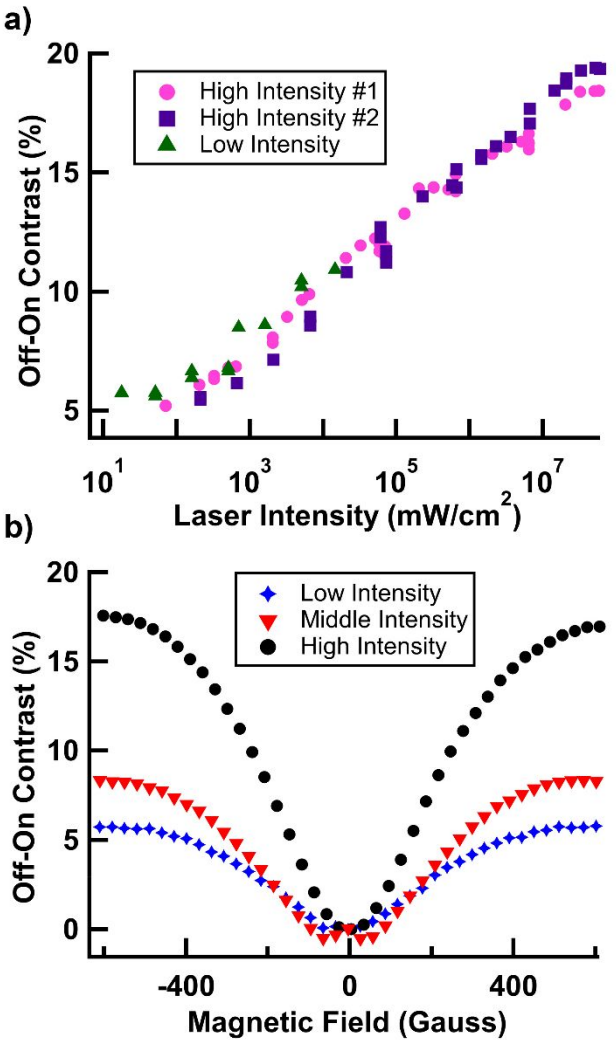

Figure 3. a) Magnet-induced contrast as a function of excitation intensity in 40 nm NVND. b) Contrast as a function of magnetic field strength under low (51 mW/cm^2), moderate (7 W/cm^2), and high (6000 W/cm^2) excitation intensity.

contrast at varying illumination intensities over six orders of magnitude. **Figure 3a** represents the results of three separate measurements: one spanning the lower illumination intensities, and two spanning the higher intensities, to ensure that contrast measurements are reproduced when illumination conditions are the same. Under our conditions the percent contrast achievable increases with illumination intensity, reaching 19% at intensities on the order of 10^7 mW/cm^2. This behavior is consistent with observations in literature, and has been explained by considering the competing rates of optical excitation in comparison with spin lattice relaxation rates and intersystem crossing rates.[34, 37] While these results imply that maximizing illumination intensity will maximize magnet-induced contrast, the likelihood of high laser intensities inducing damage and sample heating limit the practical use of such high intensities and must be considered based on the imaging application.

We also tested the effects of varying magnetic field strength on achievable fluorescence contrast using 40 nm NVND. Since both magnetic field strength and illumination intensity effect the populations of spin states in the NV center,[34, 35, 37] we

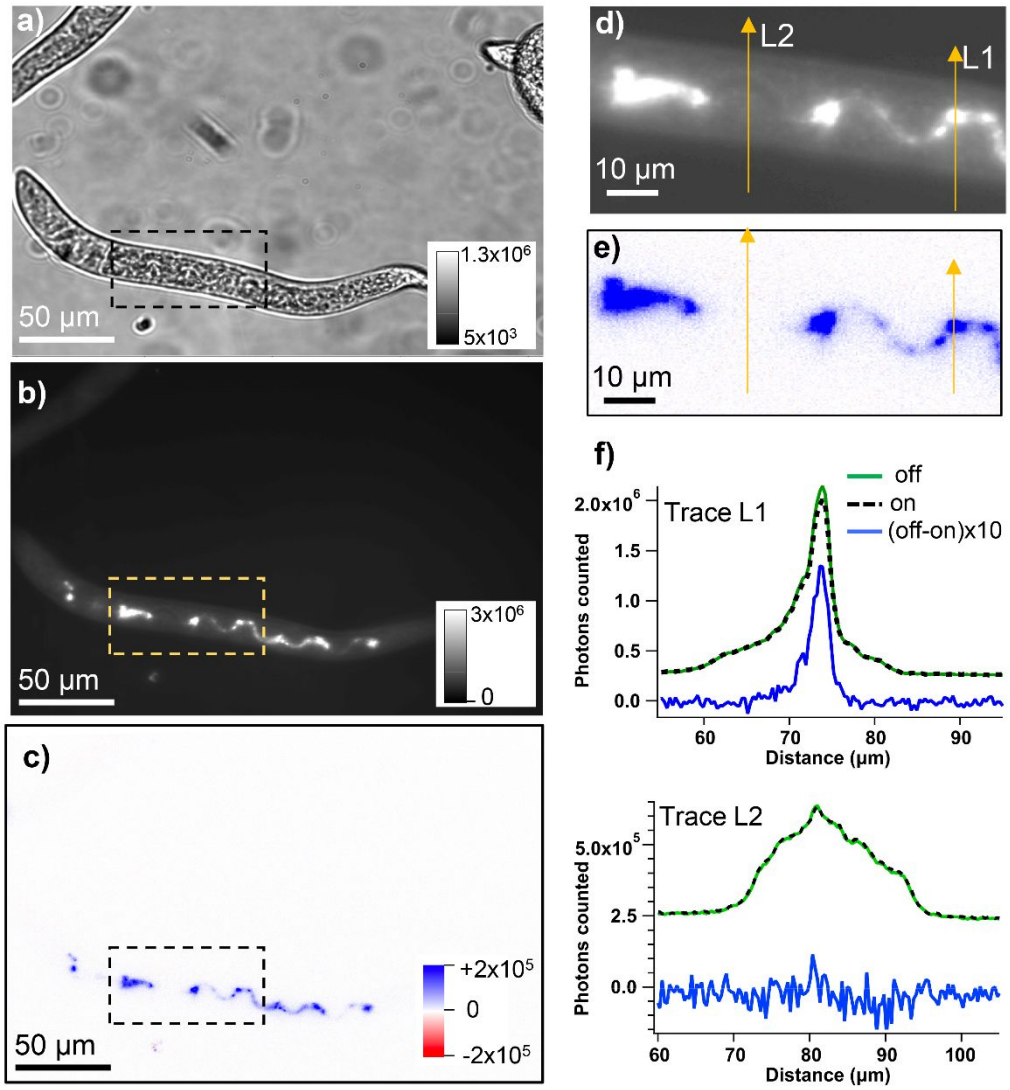

Figure 4. Imaging results of NVND exposed *C. elegans*. a) Bright-field image. b) Fluorescence image, sum of 10 individual frames. c) Image resulting from image subtraction using equation #1. d, e) Selected-area images of fluorescence and difference images. f) Line traces across the regions indicated in Figure 4d and 4e.

studied magnetic-dependent fluorescence contrast under low, moderate, and high illumination intensity (**Figure 3b**). We observe similar behavior at all illumination intensities studied, where magnet off-magnet on contrast increases with increasing magnetic field, reaching a maximum near 500 gauss. The difference in the three traces is the maximum contrast achieved, corresponding to about 17% at high illumination intensity, 8% at moderate intensity, and 5% at low intensity, which agree with the data in **Fig. 2a** which was measured nearest to the moderate illumination intensity. For reference of scale, common magnetic fields for magnetic resonance imaging in a clinical setting are on the order of 1 tesla (10,000 gauss), well above the level of the fields applied in this study.[45] The collection of data in **Figure 3** indicate that the optimum conditions for high fluorescence contrast between magnet off and magnet on conditions include applied magnetic fields greater than 500 G and high laser intensity.

Selective NV Imaging Using Differential Magnet-Induced Contrast.

To demonstrate the use of magnetic field-induced imaging contrast to identify nanomaterials within biological organisms, we conducted studies using *C. elegans* as a model organism. *C. elegans* have been shown to ingest nanoparticles that have been placed on their growth medium with the bacteria that the organism feeds on. As such, when fluorescent nanodiamond is present in the growth medium, the organisms can ingest the nanodiamond which may then be taken up into the intestinal lumen and cross into surrounding tissue.[15] Based on the size dependence of the fluorescence modulation in NV nanodiamond discussed above, we selected 40 nm diameter nanoparticles for organism exposure as a compromise between small size and high modulation contrast. Using the same optical system, we directed the fluorescence to a high-sensitivity electron-multiplying CCD (EMCCD) array instead of the SPCM and collected a series of 20 images, interleaving images with B=0 and B=400 Gauss. **Figure 4a** shows a brightfield image with one complete organism and parts of other organisms at the top

right and top left. **Figure 4b** shows the corresponding fluorescence image, collected at all wavelengths >550 nm to the wavelength limit of the CCD array (approximately 750 nm). The image in Figure 4b is the sum of 10 images with B=0. Figure 4b shows small regions of high fluorescence intensity from within the intestine of the *C. elegans*, with weaker emission visible from the elsewhere in the organism. Additional control experiments using *C. elegans* that were not exposed to nanodiamond showed autofluorescence in various regions but did not show evidence for nanodiamond in the gut region. All *C. elegans* imaged, both those exposed to nanodiamond and those not exposed, exhibited significant autofluorescence, some of which partially bleaches on the time scale of our experiments and leads to a slowly decreasing background.

Figure 4c shows the resulting difference image obtained as:

$$(M(x,y) = \sum_{n=1}^{N} Off_n(x,y) - \sum_{n=1}^{N} On_n(x,y)) \quad (1)$$

for N=10. Since the difference between images can be positive or negative, we represent the difference image using a color map. As expected, the locations of nanodiamond result in a positive difference image, indicating that the magnetic field decreases the intensity of emission. We also separately examined the individual difference frames obtained as:

$$(M_n(x,y) = Off_n(x,y) - \frac{On_n(x,y) + On_{n+1}(x,y)}{2}) \quad (2)$$

These individual difference images appeared identical to the images shown in Figure 4c except for improvement in overall signal-to-noise in the summed image M(x,y), eq. (1).

Figure 4d and **4e** show enlarged images of the region indicated by the dashed line in Figures 4a-4c. In Figure 4d we have adjusted the contrast to more clearly show the background fluorescence that extends the width of the organism. **Figure 4f** shows line plots corresponding to the numerical values of the original data sets across the indicated region. In this case trace L1 passes directly over a bright spot that we attribute to nanodiamonds, while trace L2 passes over a region that does not show an obvious bright spot but still shows the background fluorescence. In Figure 4f, the plots of L1 with magnetic field off and magnetic field on overlap almost perfectly in most of the plot except near the peak, where the intensity with the magnetic field off is higher than that with the magnetic field on. The blue trace shows the difference between these, scaled 10x for convenience. The blue trace is narrower than both the green and the black traces, and the amplitude of the blue peak corresponds to a fractional modulation of 6.2%. In the case of trace L2, the traces with B=0 and B=400 gauss are completely overlapped. The difference (again scaled vertically 10x) shows no difference between the traces. The absence of magnetic field modulation in trace L2 shows that the fluorescence does not come from nanodiamond, but instead originates in autofluorescence of the *C. elegans*. Comparing the data from traces L1 and L2, it appears that the *C. elegans* yields approximately 5 x 10^5 detected photons. Under identical conditions, in trace L1 the diamond peak yielded 2.1 x 10^6 photons and the background (visible as the broader peak extending from ~62 μm to 82 μm) also appears to correspond to ~5 x 10^5 photons, similar to that of trace L2. If it is assumed that of the 2.1 x 10^6 photons detected at the peak of trace L1, 5 x 10^5 came from non-modulated background signals and 1.6 x10^6 came from the diamond, then the 6% modulation contrast observed in trace L1 is of comparable magnitude with the ~10% modulation of the nanodiamond intensity observed from the same size nanodiamond on a coverslip in the absence of any background. To estimate the signal-to noise ratio, we measured the RMS noise in trace L1 between 85 and 95 μm, and by this method determined a signal-to-noise ratio for the difference signal (blue trace) of 13.

While the practical limit of detection will depend on the sample and the imaging conditions, an absolute limit of detection can be obtained assuming Poisson counting statistics and the 10% modulation observed in Fig. 2. Assuming C_{off} and C_{on} are the number of photons collected with magnet off and on, respectively, the Poisson noise would be $Noise = \sqrt{C_{off} + C_{on}}$. Assuming a 10% modulation, a signal-to-noise ratio S/N=3 would then require approximately 1700 photons. The high count rates and good S/N observed experimentally in Fig. 4, together with this statistically limited S/N ratio, both indicate that it should be possible to achieve high quality imaging using lower concentrations and using smaller nanoparticles.

Conclusions

The ability to selectively identify nanodiamond in the presence of confounding emission from autofluorescence, scattering, and other sources of non-diamond emission can provide a unique way to leverage the quantum properties of nanodiamond for enhanced imaging applications. As demonstrated here, fractional modulations of 19% can be achieved using 40 nm nanodiamond and an inexpensive ($10 USD) electromagnet. In a practical imaging application, lower (>6%) modulation contrast measured with signal-to-noise ratio of 13 is achieved in imaging nanodiamonds ingested by *C. elegans*. As NV centers, especially those in nanodiamonds, are increasingly used in bio-imaging and sensing applications using resonant MW fields, the use of time-modulated magnetic fields offers an alternative for producing fluorescence contrast that minimizes cost, complexity of instrumentation, and sample heating associated with more elaborate schemes such as ODMR. The application of this method is straightforward in common imaging systems and may be of great use in identifying uptake of nanoparticles by organisms under conditions relevant to understanding the environmental impact of nanomaterials.

Conflicts of interest

There are no conflicts to declare.

Acknowledgements

This work was supported by the National Science Foundation, the Center for Sustainable Nanotechnology (CSN), CHE-1503408. The CSN is part of the Centers for Chemical Innovation Program. Collaboration between ZRJ and OS was augmented by support from NSF award DMR-1747426.

References

1. X. Y. Ou, Y. Y. Chen, L. L. Xie, J. Chen, J. Zan, X. F. Chen, Z. Z. Hong, Y. He, J. Li and H. H. Yang, X-ray Nanocrystal Scintillator-Based Aptasensor for Autofluorescence-Free Detection, *Analytical Chemistry*, 2019, **91**, 10149-10155.
2. B. R. Smith and S. S. Gambhir, Nanomaterials for In Vivo Imaging, *Chemical Reviews*, 2017, **117**, 901-986.
3. F. von der Kammer, P. L. Ferguson, P. A. Holden, A. Masion, K. R. Rogers, S. J. Klaine, A. A. Koelmans, N. Horne and J. M. Unrine, Analysis of engineered nanomaterials in complex matrices (environment and biota): General considerations and conceptual case studies, *Environmental Toxicology and Chemistry*, 2012, **31**, 32-49.
4. M. Hassellov, J. W. Readman, J. F. Ranville and K. Tiede, Nanoparticle analysis and characterization methodologies in environmental risk assessment of engineered nanoparticles, *Ecotoxicology*, 2008, **17**, 344-361.
5. N. Billinton and A. W. Knight, Seeing the wood through the trees: A review of techniques for distinguishing green fluorescent protein from endogenous autofluorescence, *Analytical Biochemistry*, 2001, **291**, 175-197.
6. O. S. Wolfbeis, An overview of nanoparticles commonly used in fluorescent bioimaging, *Chemical Society Reviews*, 2015, **44**, 4743-4768.
7. E. R. Wilson, L. M. Parker, A. Orth, N. Nunn, M. D. Torelli, O. Shenderova, B. Gibson and P. Reineck, The effect of particle size on nanodiamond fluorescence and colloidal properties in biological media, *Nanotechnology*, 2019, **30**, 385704.
8. M. D. S. Pena, A. Gottipati, S. Tahiliani, N. M. Neu-Baker, M. D. Frame, A. J. Friedman and S. A. Brenner, Hyperspectral Imaging of Nanoparticles in Biological Samples: Simultaneous Visualization and Elemental Identification, *Microscopy Research and Technique*, 2016, **79**, 349-358.
9. E. Wild and K. C. Jones, Novel Method for the Direct Visualization of in Vivo Nanomaterials and Chemical Interactions in Plants, *Environmental Science & Technology*, 2009, **43**, 5290-5294.
10. P. Reineck and B. C. Gibson, Near-Infrared Fluorescent Nanomaterials for Bioimaging and Sensing, *Advanced Optical Materials*, 2017, **5**.
11. Z.-J. Zhu, Y.-C. Yeh, R. Tang, B. Yan, J. Tamayo, R. W. Vachet and V. M. Rotello, Stability of quantum dots in live cells, *Nature Chemistry*, 2011, **3**, 963.
12. Z. G. Wang, S. L. Liu, Y. J. Hu, Z. Q. Tian, B. Hu, Z. L. Zhang and D. W. Pang, Dissecting the Factors Affecting the Fluorescence Stability of Quantum Dots in Live Cells, *Acs Applied Materials & Interfaces*, 2016, **8**, 8401-8408.
13. B. Zhi, Y. Cui, S. Y. Wang, B. P. Frank, D. N. Williams, R. P. Brown, E. S. Melby, R. J. Hamers, Z. Rosenzweig, D. H. Fairbrother, G. Orr and C. L. Haynes, Malic Acid Carbon Dots: From Super-resolution Live-Cell Imaging to Highly Efficient Separation, *Acs Nano*, 2018, **12**, 5741-5752.
14. W. W. W. Hsiao, Y. Y. Hui, P. C. Tsai and H. C. Chang, Fluorescent Nanodiamond: A Versatile Tool for Long-Term Cell Tracking, Super-Resolution Imaging, and Nanoscale Temperature Sensing, *Accounts of Chemical Research*, 2016, **49**, 400-407.
15. N. Mohan, C. S. Chen, H. H. Hsieh, Y. C. Wu and H. C. Chang, In vivo imaging and toxicity assessments of fluorescent nanodiamonds in caenorhabditis elegans, *Nano Letters*, 2010, **10**, 3692-3699.
16. D. A. Simpson, A. J. Thompson, M. Kowarsky, N. F. Zeeshan, M. S. J. Barson, L. T. Hall, Y. Yan, S. Kaufmann, B. C. Johnson, T. Ohshima, F. Caruso, R. E. Scholten, R. B. Saint, M. J. Murray and L. C. L. Hollenberg, In vivo imaging and tracking of individual nanodiamonds in drosophila melanogaster embryos, *Biomedical Optics Express*, 2014, **5**, 1250.
17. L. Childress and R. Hanson, Diamond NV centers for quantum computing and quantum networks, *MRS Bulletin*, 2013, **38**, 134-138.
18. E. Abe and K. Sasaki, Tutorial: Magnetic resonance with nitrogen-vacancy centers in diamond - Microwave engineering, materials science, and magnetometry, *Journal of Applied Physics*, 2018, **123**, 161101.
19. C. L. Degen, F. Reinhard and P. Cappellaro, Quantum sensing, *Reviews of Modern Physics*, 2017, **89**.
20. S. Kaufmann, D. A. Simpson, L. T. Hall, V. Perunicic, P. Senn, S. Steinert, L. P. McGuinness, B. C. Johnson, T. Ohshima, F. Caruso, J. Wrachtrup, R. E. Scholten, P. Mulvaney and L. Hollenberg, Detection of atomic spin labels in a lipid bilayer using a single-spin nanodiamond probe, *Proceedings of the National Academy of Sciences*, 2013, **110**, 10894-10898.
21. J. R. Maze, P. L. Stanwix, J. S. Hodges, S. Hong, J. M. Taylor, P. Cappellaro, L. Jiang, M. V. G. Dutt, E. Togan, A. S. Zibrov, A. Yacoby, R. L. Walsworth and M. D. Lukin, Nanoscale magnetic sensing with an individual electronic spin in diamond, *Nature*, 2008, **455**, 644-647.
22. R. Schirhagl, K. Chang, M. Loretz and C. L. Degen, Nitrogen-Vacancy Centers in Diamond: Nanoscale Sensors for Physics and Biology, *Annual Review of Physical Chemistry*, 2014, **65**, 83-105.
23. N. Nunn, M. Torelli, G. McGuire and O. Shenderova, Nanodiamond: A high impact nanomaterial.*Journal*, 2017, **21**, 1-9.
24. P. Reineck, A. Francis, A. Orth, D. W. M. Lau, R. D. V. Nixon-Luke, I. D. Rastogi, W. A. W. Razali, N. M. Cordina, L. M. Parker, V. K. A. Sreenivasan, L. J. Brown and B. C. Gibson, Brightness and Photostability of Emerging Red and Near-IR Fluorescent Nanomaterials for Bioimaging, *Advanced Optical Materials*, 2016, **4**, 1549-1557.
25. J. M. Say, C. van Vreden, D. J. Reilly, L. J. Brown, J. R. Rabeau and N. J. C. King, Luminescent nanodiamonds for biomedical applications, *Biophysical Reviews*, 2011, **3**, 171-184.
26. O. Shenderova, N. Nunn, T. Oeckinghaus, M. Torelli, G. McGuire, K. Smith, E. Danilov, R. Reuter, J. Wrachtrup, A. Shames, D. Filonova and A. Kinev, Proceedings Volume 10118, Advances in Photonics of Quantum Computing, Memory, and Communication X, 2017.
27. K. van der Laan, M. Hasani, T. Zheng and R. Schirhagl, Nanodiamonds for In Vivo Applications, *Small*, 2018, **14**, 1703838.

28. C. Stavis, T. L. Clare, J. E. Butler, A. D. Radadia, R. Carr, H. J. Zeng, W. P. King, J. A. Carlisle, A. Aksimentiev, R. Bashir and R. J. Hamers, Surface functionalization of thin-film diamond for highly stable and selective biological interfaces, *Proceedings of the National Academy of Sciences of the United States of America*, 2011, **108**, 983-988.
29. W. S. Yang, O. Auciello, J. E. Butler, W. Cai, J. A. Carlisle, J. Gerbi, D. M. Gruen, T. Knickerbocker, T. L. Lasseter, J. N. Russell, L. M. Smith and R. J. Hamers, DNA-modified nanocrystalline diamond thin-films as stable, biologically active substrates, *Nature Materials*, 2002, **1**, 253-257.
30. M. W. Doherty, N. B. Manson, P. Delaney, F. Jelezko, J. Wrachtrup and L. C. L. Hollenberg, The nitrogen-vacancy colour centre in diamond, *Physics Reports*, 2013, **528**, 1-45.
31. A. Gruber, A. Dräbenstedt, C. Tietz, L. Fleury, J. Wrachtrup and C. Von Borczyskowski, Scanning confocal optical microscopy and magnetic resonance on single defect centers, *Science*, 1997, **276**, 2012-2014.
32. R. Igarashi, Y. Yoshinari, H. Yokota, T. Sugi, F. Sugihara, K. Ikeda, H. Sumiya, S. Tsuji, I. Mori, H. Tochio, Y. Harada and M. Shirakawa, Real-time background-free selective imaging of fluorescent nanodiamonds in vivo, *Nano Letters*, 2012, **12**, 5726-5732.
33. M. E. Robinson, J. D. Ng, H. Zhang, J. T. Buchman, O. A. Shenderova, C. L. Haynes, Z. Ma, R. H. Goldsmith and R. J. Hamers, Optically detected magnetic resonance for selective imaging of diamond nanoparticles, *Analytical Chemistry*, 2017, **90**, 769-776.
34. M. Capelli, P. Reineck, D. W. M. Lau, A. Orth, J. Jeske, M. W. Doherty, T. Ohshima, A. D. Greentree and B. C. Gibson, Magnetic field-induced enhancement of the nitrogen-vacancy fluorescence quantum yield, *Nanoscale*, 2017, **9**, 9299-9304.
35. R. J. Epstein, F. M. Mendoza, Y. K. Kato and D. D. Awschalom, Anisotropic interactions of a single spin and dark-spin spectroscopy in diamond, *Nature Physics*, 2005, **1**, 94-98.
36. N. D. Lai, D. Zheng, F. Jelezko, F. Treussart and J. F. Roch, Influence of a static magnetic field on the photoluminescence of an ensemble of nitrogen-vacancy color centers in a diamond single-crystal, *Applied Physics Letters*, 2009, **95**, 133101.
37. S. K. R. Singam, J. Motylewski, A. Monaco, E. Gjorgievska, E. Bourgeois, M. Nesládek, M. Giugliano and E. Goovaerts, Contrast Induced by a Static Magnetic Field for Improved Detection in Nanodiamond Fluorescence Microscopy, *Physical Review Applied*, 2016, **6**.
38. J. P. Tetienne, L. Rondin, P. Spinicelli, M. Chipaux, T. Debuisschert, J. F. Roch and V. Jacques, Magnetic-field-dependent photodynamics of single NV defects in diamond: An application to qualitative all-optical magnetic imaging, *New Journal of Physics*, 2012, **14**, 103033.
39. R. Chapman and T. Plakhoitnik, Background-free imaging of luminescent nanodiamonds using external magnetic field for contrast enhancement, *Optics Letters*, 2013, **38**, 1847.
40. S. K. Sarkar, A. Bumb, X. Wu, K. A. Sochacki, P. Kellman, M. W. Brechbiel and K. C. Neuman, Wide-field in vivo background free imaging by selective magnetic modulation of nanodiamond fluorescence, *Biomedical Optics Express*, 2014, **5**, 1190.
41. L.-J. Su, M.-S. Wu, Y. Y. Hui, B.-M. Chang, L. Pan, P.-C. Hsu, Y.-T. Chen, H.-N. Ho, Y.-H. Huang, T.-Y. Ling, H.-H. Hsu and H.-C. Chang, Fluorescent nanodiamonds enable quantitative tracking of human mesenchymal stem cells in miniature pigs, *Scientific Reports*, 2017, **7**, 45607.
42. T. Stiernagle, Maintenance of C. elegans, *WormBook*, 2006, DOI: 10.1895/wormbook.1.101.1.
43. V. Petráková, A. Taylor, I. Kratochvílová, F. Fendrych, J. Vacík, J. Kučka, J. Štursa, P. Cígler, M. Ledvina, A. Fišerová, P. Kneppo and M. Nesládek, Luminescence of nanodiamond driven by atomic functionalization: Towards novel detection principles, *Advanced Functional Materials*, 2012, **22**, 812-819.
44. L. Rondin, G. Dantelle, A. Slablab, F. Grosshans, F. Treussart, P. Bergonzo, S. Perruchas, T. Gacoin, M. Chaigneau, H. C. Chang, V. Jacques and J. F. Roch, Surface-induced charge state conversion of nitrogen-vacancy defects in nanodiamonds, *Physical Review B: Condensed Matter*, 2010, **82**, 115449.
45. A. Berger, Magnetic resonance imaging, *The British Medical Journal*, 2002, **324**, 35.

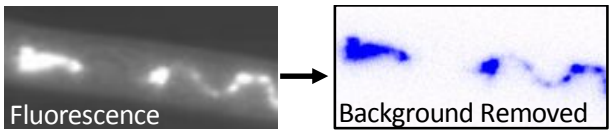

The unique properties of NV centers in diamond nanoparticles enable selective identification within organisms and other complex environmental matrices